Statistics-tuned phases of pseudofermions in one dimension

Adhip Agarwala,[1,*] Gaurav Kumar Gupta,[2,†] Vijay B. Shenoy,[2,‡] and Subhro Bhattacharjee[1,§]
[1]*International Centre for Theoretical Sciences, Tata Institute of Fundamental Research, Bengaluru 560089, India*
[2]*Centre for Condensed Matter Theory, Department of Physics, Indian Institute of Science, Bangalore 560 012, India*

(Received 19 December 2018; revised manuscript received 24 March 2019; published 17 April 2019)

We show that a quadratic system of *pseudofermions*, with tunable fractionalized statistics, can host a rich phase diagram on a one-dimensional chain with nearest- and next-nearest-neighbor hopping. Using a combination of numerical and analytical techniques, we show that by varying the statistical angle and the ratio of the hopping, the system stabilizes two Tomonaga-Luttinger liquids (TLL) with central charges $c = 1$ and 2, respectively, along with the inversion symmetry broken bond-ordered (BO) insulating phase. Interestingly, the two quantum phase transitions in the system, (1) between the two TLLs and (2) the $c = 1$ TLL and BO phase, can be engendered by solely tuning the statistics of the pseudofermions. Our analysis shows that both these transitions are continuous and novel with the former lacking a local order-parameter based description and the latter of Berezinskii-Kosterlitz-Thouless type. These phases and phase transitions can be of direct experimental relevance in the context of recent studies of fermionic cold atoms.

DOI: 10.1103/PhysRevB.99.165125

I. INTRODUCTION

Advances in the physics of one-dimensional systems motivated by, *inter alia*, the possibility of Majorana zero modes [1–3], have ushered in many new possibilities and opportunities. Particularly remarkable is the prospect of creating quantum entangled phases with fractional quantum numbers and statistics [4–9]. Several recent proposals indeed suggest that starting with bosons or fermions, effective local Hamiltonians with degrees of freedom following *fractionalized* or *intermediate* statistics can be realized, for example, in ultracold atomic systems [10–14]. Exploring the physics of such a system with tunable statistics has hence emerged as an active field of research.

One way of tuning statistics can be accomplished by generalizing the commutation algebra of second quantized creation/annihilation operators between different sites on a one-dimensional chain via a parameter ϕ such that at $\phi = 0$ one realizes "fermions" and at $\phi = \pi$ "bosons." This however still allows for a freedom to choose on-site operators to be either bosonic or fermionic. We call the former choice as *pseudobosons* and the latter as *pseudofermions*. Both pseudobosons and pseudofermions are generalizations of two-dimensional "anyons" to one spatial dimension following the pioneering work of Leinass and Myrheim [4]. In fact, early works on exactly solvable one-dimensional interacting bosonic [5,6] and fermionic systems [7–9] have shown interesting implications on generalized operator algebra [15–18] as well as understanding of such one-dimensional anyons in terms of exclusion statistics [19] and generalized distribution functions [20,21].

Recent work, in particular motivated by the advances in ^{87}Rb cold atomic experiments [22–25], has concentrated on pseudobosons [12,26–35]. However, even more recently, there have been crucial experimental breakthroughs in cold atomic experiments with fermionic atoms. This includes, among other things, realization of spin-orbit coupling in ^{87}Sr [36] atoms, and spin-dependent tunneling and correlated hopping in ^{40}K atoms [37–39]. Indeed, several interacting *many-body phases* such as correlated insulators [40,41], incommensurate magnets [42], and topological phases have been realized [43,44].

In parallel, several microscopic lattice Hamiltonians with tunable couplings have been realized in optical lattice setups of ^{173}Yb [45,46] atoms, such as the Creutz ladder [47] and the cross-linked chiral ladder [48]. This opens the possibility to explore, as we show below, a very different, but equally rich set of somewhat complementary set of phases and associated unconventional quantum phase transitions for the pseudofermions.

In this paper we introduce a deceptively simple hopping problem of pseudofermions on a *zigzag ladder* and show that it can realize many interesting phases and phase transitions. This hopping problem is parametrized by a single dimensionless parameter t_2/t_1 which is the ratio of hopping strengths between the next-nearest-neighbor and nearest-neighboring sites (see Fig. 1) in addition to an angle $\phi \in [0, \pi]$ that characterizes the statistics of pseudofermions themselves. Interestingly we show that the above pseudofermion hopping problem is equivalent to a correlated hopping model for fermions in one dimension. Hence our results can be alternatively looked upon as an outcome of competing interactions mediated by constrained kinetic energy, characteristic to strongly correlated solid-state systems [49–52]. The central result of this work is summarized in Fig. 2 which shows the various phases

*adhip.agarwala@icts.res.in
†ggaurav@iisc.ac.in; Present address: Physics Department, Technion, 32000 Haifa, Israel.
‡shenoy@iisc.ac.in
§subhro@icts.res.in

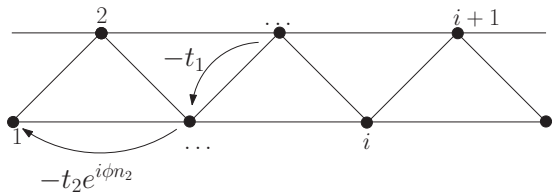

FIG. 1. Model Hamiltonian: Schematic figure describing a pseudofermion hopping model, or equivalently the correlated fermionic hopping Hamiltonian [see Eqs. (2) and (4)] on a zigzag chain.

and phase transitions realizable in this system. In particular, phases realized include an inversion symmetry broken gapped bond-ordered (BO) phase in addition to the two Tomonaga-Luttinger liquids (TLL) with central charges $c = 1$ and $c = 2$, respectively. Most interestingly, both as a function of the hopping amplitudes as well as the statistical angle ϕ, the pseudofermions show direct *Lifshitz* phase transition [53–56] between $c = 1$ and $c = 2$ TLLs. This Lifshitz transition thus provides an example of a phase transition between two non-Fermi liquids each of which is described by separate conformal field theories (CFTs). Furthermore, in a regime of t_2/t_1, another unconventional continuous quantum phase transition can be engendered by *tuning the statistical parameter* ϕ between the $c = 1$ TLL and the BO phase. This latter transition is of Berezinskii-Kosterlitz-Thouless (BKT) type with subtle *Berry phase* effects leading to inversion symmetry broken BO phase.

We provide a comprehensive understanding of the phase diagram using a combination of approaches such as density matrix renormalization group (DMRG) (corroborated numerically with exact diagonalization for smaller system sizes), Hartree-Fock (HF) theory, and bosonization approaches. Our results can motivate further experimental work, particularly in cold atoms to pursue some of these interesting phases and phase transitions.

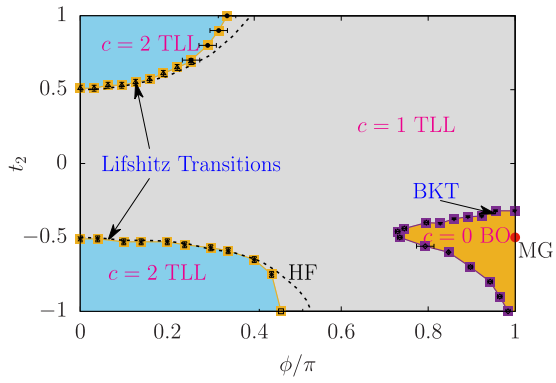

FIG. 2. Phase diagram: Phases of the model in the ϕ-t_2 plane ($t_1 = 1$). At $\phi = 0$ the free Fermi system encounters Lifshitz transitions where the number of Fermi points changes. At $\phi \neq 0$ these evolve into central charge $c = 1$ and $= 2$ Tomonaga-Luttinger liquids (TLL). Near $\phi = \pi$ systems undergo a BKT transition from $c = 1$ TLL to a gapped bond-ordered (BO) phase which spontaneously breaks lattice parity. At $\phi = \pi$ and $t_2 = -0.5$ the system has an exactly solvable Majumdar-Ghosh (MG) point. The phase boundaries are determined by studying the excitation gap. The dashed line represents the Lifshtiz transitions under the Hartree-Fock (HF) approximation (see text). Representative system sizes for DMRG calculations are $L \sim 200$.

The rest of the paper is arranged as follows.

In Sec. II we introduce the idea of generalized algebra and the Hamiltonian we are interested in (with further details on the symmetries in Appendix A). In Sec. III we uncover the rich phase diagram of the model using various methods. Section III A first discusses free fermion limit and explicitly shows how the Hartree-Fock solution predicts that the TLL ($c = 1$) to TLL ($c = 2$) gapless-gapless transition is indeed a Lifshitz transition even in the interacting regime. Section III B further analyzes the model using DMRG and characterizes the various phases and phase transitions through scaling of the excitation gap, nature of fidelity, and central charge. Some of the numerical details are relegated to Appendix D. In order to further understand the phases and the phase transitions we include fluctuations over the HF ground state under bosonization framework. This analysis is presented in Sec. IV. Here we also provide comprehensive understanding of the TLL phase and the dependence of the Luttinger parameter K on ϕ both from DMRG and bosonization. In Sec. V we summarize our results and provide the possibility of realizing this experimentally in cold atomic experiments with fermionic atoms.

II. GENERALIZED ALGEBRA: PSEUDOFERMIONS IN ONE DIMENSION

In a one-dimensional (1D) chain with sites labeled i, j, etc., tunable statistics can be captured by the algebra generated by the on-site creation/annihilation operators given by

$$\begin{aligned} a_j a_i \pm a_i a_j e^{\mathbb{i}\phi\,\mathrm{sgn}(i-j)} &= 0, \\ a_j a_i^\dagger \pm a_i^\dagger a_j e^{-\mathbb{i}\phi\,\mathrm{sgn}(i-j)} &= \delta_{ij}, \\ [N_i, a_j] &= -\delta_{ij} a_j, \\ [N_i, a_j^\dagger] &= \delta_{ij} a_j^\dagger \end{aligned} \tag{1}$$

(where $N_i = a_i^\dagger a_i$). The underlying physics consistent with $\mathrm{sgn}(0) = 0$ produces an on-site algebra that is bosonic or fermionic depending on the relative sign ($\pm$). Owing to this, we refer to the two cases as pseudofermions ($+$ sign) or pseudobosons ($-$ sign), respectively, even for $\phi \neq 0$. In either case, the off-site algebra can be tuned from fermionic to bosonic (or vice versa) by an appropriately tuning *statistical parameter* $\phi \in [0, \pi]$. However pseudofermions, unlike pseudobosons, satisfy a hard-core constraint at *any* ϕ with $\phi = \pi$ limit being the hard-core boson limit. While this constraint may also be accessed as the infinite on-site interaction limit of pseudobosons, pseudofermions are naturally relevant to studies of ultracold fermionic atoms [57,58] and hence can allow us access to complementary parts of the generalized phase diagram.

To this end, we consider a set of pseudofermions hopping on a one-dimensional lattice labeled by sites i via the

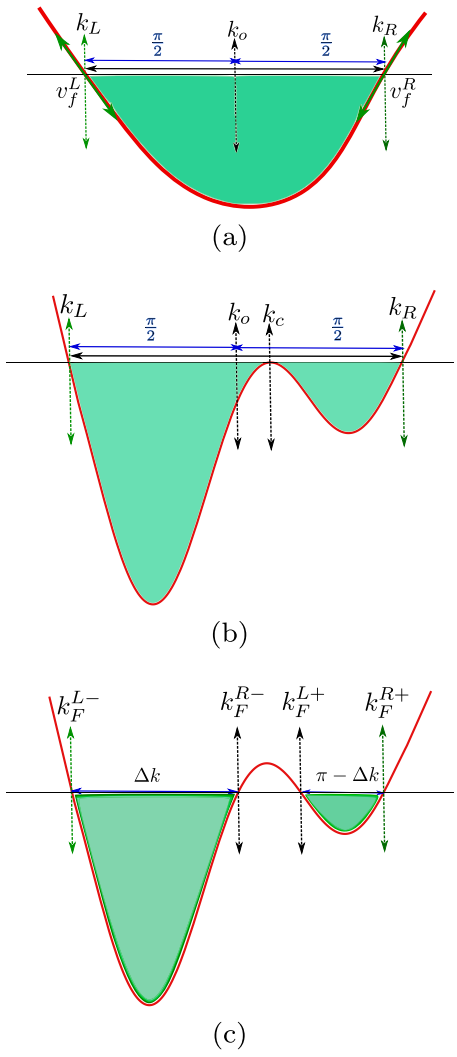

FIG. 3. Lifshitz transition schematically: (a) The Hartree-Fock (HF) dispersion is schematically shown in the TLL $c = 1$ phase. (b) Schematic of the HF dispersion at a "Lifshitz" transition when the system undergoes a gapless-gapless transition between TLL ($c = 1$) and TLL ($c = 2$) phase. (c) Schematic of the HF dispersion when the system is in $c = 2$ TLL phase.

Hamiltonian

$$H = -\sum_i [t_1 a_i^\dagger a_{i+1} + t_2\, a_i^\dagger a_{i+2}] + \text{H.c.}, \tag{2}$$

where t_1 (t_2) denotes the nearest- (next-nearest-) neighbor hopping. We focus on half-filling and this model, as we will discuss below, has a rich phase diagram (see Fig. 2) with interesting gapless and gapped phases.

To uncover the physics of Eq. (2) we exploit the well known idea of interchanging statistics and interactions in 1D by introducing fractional Jordan-Wigner strings K_i, and defining operators

$$c_i = K_i a_i, \quad c_i^\dagger = a_i^\dagger K_i^\dagger \quad \text{with} \quad K_i = e^{-\mathbb{i}\phi \sum_{j<i} n_j}. \tag{3}$$

Equation (2) is thus mapped into a *fermionic* Hamiltonian

$$\mathcal{H} = -\sum_i [t_1 c_i^\dagger c_{i+1} + t_2 e^{\mathbb{i}\phi n_{i+1}} c_i^\dagger c_{i+2}] + \text{H.c.}, \tag{4}$$

where $c_i^\dagger, c_i$ are fermionic creation/annihilation operators at site i obeying usual fermion anticommutation algebra with the number density $n_i = c_i^\dagger c_i$. While the first term in Eq. (4) is the nearest-neighbor hopping, the second term contains the physics of *correlated hopping* between next-nearest-neighboring sites—fermions hop with a phase of 0 (ϕ) in the absence (presence) of another fermion at the intermediate site (see Fig. 1). We note that a finite t_2 is crucial to realization of nontrivial phases [59,60]. Interestingly, correlated hoppings are known to arise in strongly correlated systems with constrained kinetic energies leading to frustration [49–52,61]. In particular, correlated hoppings can lead to unconventional superconductivity [50,51,62,63] and many-body bound states [52,64]. Interestingly, recent work has shown that correlated hoppings can realize topological phases such as integer quantum Hall effect of bosons [65].

At $\phi = 0$ and π, the Hamiltonian in Eq. (4) has both time-reversal (TRS) and parity symmetries separately present. At any generic ϕ only a combination of both is a symmetry (for a detailed discussion on the symmetries see Appendix A). Under the nonlocal transformation [see Eq. (3)] the pseudofermion number density operator $N_i = a_i^\dagger a_i$ is equal to the fermion density operator $n_i = c_i^\dagger c_i$ and hence the *filling fraction* remains unchanged and the system conserves the total number of particles. Here we shall focus on 1/2 filling. In the remainder we set $t_1 = 1$ and study the phase diagram as a function of t_2 (real) and ϕ. The system described in Eq. (4) is studied by analytical and numerical techniques.

III. PHASE DIAGRAM

A. Mean field theory around ($\phi = 0$) free fermionic limit

1. $\phi = 0$: *free fermions*

Along the $\phi = 0$ line the system reduces to that of free fermions with nearest- and next-nearest-neighbor hopping with a single particle dispersion given by

$$E(k) = -2t_1 \cos k - 2t_2 \cos 2k, \quad k \in [-\pi, \pi]. \tag{5}$$

Due to parity for $\phi = 0$, the dispersion is always symmetric about $k \to -k$. There is a change in the number of the Fermi points as the system undergoes a Lifshitz transition at $t_2/t_1 = \pm 0.5$. For $|t_2/t_1| > 0.5$ (< 0.5), there are four (two) Fermi points corresponding to the left most extremum of Fig. 2 (see details in Appendix B).

2. *Self-consistent Hartree-Fock theory*

The Hartree-Fock (HF) theory incorporates the effect of the interactions *on average*. This starts by writing the fermionic Hamiltonian in Eq. (4) (in Fourier space) as a sum of the free quadratic part and an interacting quartic part:

$$H = H_0 + H_{\text{int}}, \tag{6}$$

where in the momentum space $k \in [-\pi, \pi]$, and

$$H_0 = \sum_k \varepsilon_0(k) c_k^\dagger c_k \tag{7}$$

being the (free) quadratic part with

$$\varepsilon_0(k) = -2[t \cos(k) + t_2 \cos(2k)]$$

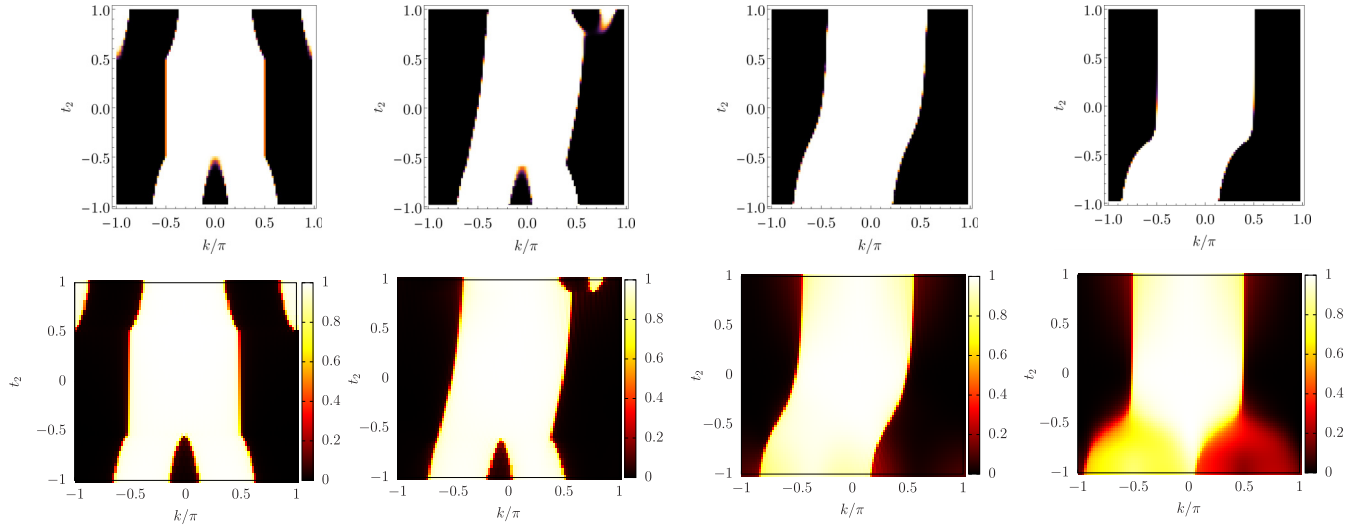

FIG. 4. Fermionic occupancy using HF and DMRG: $\langle n(k)\rangle$ as a function of k and t_2 for different values of $\phi = 0.0, 1.0, 2.0, 3.0$ using self-consistent mean field theory (top panel) and DMRG calculations (bottom panel) ($L = 62$).

being the bare dispersion and

$$H_{\text{int}} = -t_2 \sum_{k_1,k_2,k_3,k_4} \delta(k_1 + k_2 - k_3 - k_4) \times [(e^{i\phi} - 1)e^{i(-k_2+k_3+2k_4)}] \times c^\dagger_{k_1} c^\dagger_{k_2} c_{k_3} c_{k_4} + \text{H.c.} \quad (8)$$

Within a self-consistent HF treatment of the correlated hopping term (for $\phi \neq 0$) we decouple the k-mode density $\langle n(k)\rangle = \langle c^\dagger_k c_k\rangle$ as discussed in Appendix C.

The general structure of the HF band is shown schematically in Fig. 3 when the system is in the two kinds of TLL phases and at a Lifshitz transition. We find that for $|t_2/t_1| < 0.5$, the center of the Fermi surface shifts away from zero for $\phi \neq 0, \pi$ due to the absence of TRS. For higher values of $|t_2/t_1|$ the Lifshitz transition continues into the $\phi \neq 0$ regime. Figure 4 shows the HF fermionic occupation for representative points in the parameter space. The HF theory clearly captures the gapless phases with two and four Fermi points as well as an associated Lifshitz phase transition separating the two. For comparison we have also plotted the fermionic occupation $\langle n(k)\rangle$ for the fermions obtained from our DMRG calculations in Fig. 4. Clearly there is a good quantitative agreement on the position of the Fermi points such that fluctuations on top of the HF theory can be systematically incorporated within Abelian bosonization approaches as presented below. The Lifshitz transitions of this effective HF Hamiltonian at any $\{t_2, \phi\}$ traces a continuous quantum phase transition between the two gapless metallic phases (see the dashed curve in Fig. 2). However, not unexpectedly, this HF analysis breaks down in the gapped phase obtained in the vicinity of $\phi = \pi$.

B. DMRG results

To understand the nature of the phases and phase transitions beyond HF theory, we performed density matrix renormalization group (DMRG) (using [66]) on Eq. (4). Here we provide various details of our DMRG calculations including the comparison with exact diagonalization (ED) results for small systems.

1. The metallic phases: Tomonaga-Luttinger liquid metals

The DMRG calculations incorporate the fluctuations ignored in the HF theory. Once these fluctuations are incorporated, two metallic TLL phases occupy the phase diagram (see Fig. 2) for ϕ away from π. We calculate the single particle excitation gap Δ_L,

$$\Delta_L = E(L, N+1) + E(L, N-1) - 2E(L, N) \quad (9)$$

[where $E(L, N)$ is the ground state energy for a system with N fermions on L sites] numerically using DMRG and systematically perform finite-size scaling. In the gapless regime Δ_L scales as $1/L$ (see Fig. 5) and reaches zero while in the gapped regime the value saturates to a finite value $\equiv \Delta_\infty$. The $\Delta_\infty = 0$ is one measure that identifies the gapless metallic region from our DMRG calculations.

Using DMRG we calculate $\langle n(k)\rangle$ for few representative parameteres as was shown in Fig. 4. While HF theory does reproduce DMRG fermion occupancy of these phases remarkably well (see Fig. 4), we must note that once the interactions are incorporated the single-particle residue is completely killed resulting in the non-Fermi liquid TLL. However, as is clear from Fig. 4, the Lifshitz transition survives in the presence of fluctuations and we indeed have two different TLLs.

In order to further understand the above fluctuations and characterize these phases further, we calculate their central charges using the Calabrese-Cardy formula for the entanglement entropy [67] (see Appendix D) from our DMRG results. This is summarized in Fig. 6 which shows that even for finite ϕ, the Lifshitz transition survives for the pseudofermions that separates two TLLs $c = 1$ and the $c = 2$ TLLs. We find that this transition can also be characterized from the "moment of intertia" of the Fermi sea given by

$$I = \int dk \langle n(k)\rangle [\sin(k)]^2, \quad (10)$$

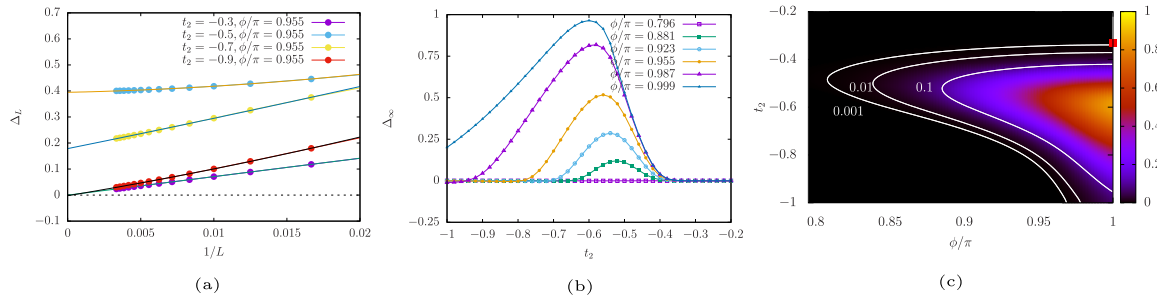

FIG. 5. Excitation gap: (a) Behavior of Δ_L at some parameters of $\{t_2, \phi\}$ as a function of $1/L$. For gapless phases Δ_L reaches zero as a function of $1/L$ and saturates to a finite value ($\equiv \Delta_\infty$) for a gapped regime. (b) Behavior of Δ_∞ in the gapped regime is shown as a function of t_2 for few values of ϕ and (c) is the same as (b) in the region.

the variation of which as a function of t_2 for different values of ϕ is shown in Fig. 7 and also in the lower panel of Fig. 6. While the gapless to gapless transition is characterized by a change in I, the gapless to gapped transition (see below) shows, as expected, no such variation.

2. Around $\phi = \pi$: The gapped phase

For $\phi = \pi$ we recover the familiar fermion to (hard-core) boson mapping evident from Eqs. (1) and (3). Thus we have a 1/2-filled system of hard-core bosons with nearest- and next-nearest-neighbor hoppings corresponding to the right extremum of Fig. 2. This is the easy-plane limit of the J_1-J_2 spin-1/2 chain [68,69]. It has two phases: $c = 1$ TLL for $t_2/t_1 \gtrsim -0.3$ and a gapped BO phase which spontaneously breaks inversion symmetry about a site. Variation of Δ_∞ as a function of t_2 for various values of ϕ is shown in Fig. 5 showing the gapped regime.

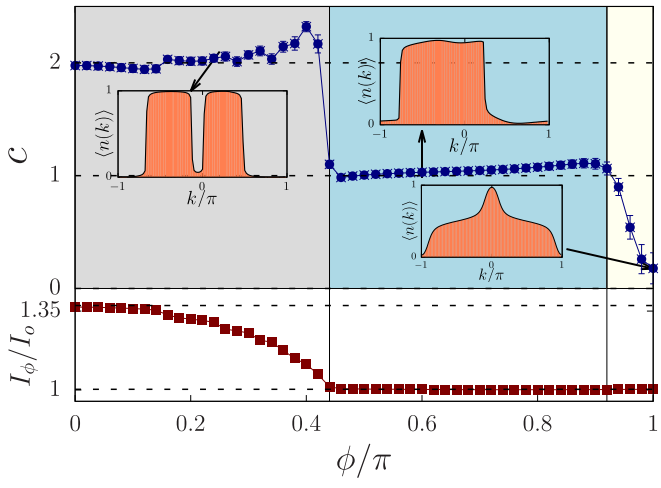

FIG. 6. Lifshitz transition: (Top) Central charge as a function of ϕ at $t_2 = -0.75$ shows a transition from a $c = 2$ to a $c = 1$ plateau. Fermion occupancy $\langle n(k)\rangle$ is shown as a function of k at three representative values of ϕ as pointed. (Bottom) Variation of $I_\phi \equiv \int_{-\pi}^{\pi} \sin^2 k \langle n(k)\rangle dk$ captures the Lifshitz transition. I_o is the corresponding value for a half-filled Fermi sea at $t_2 = 0$.

The bond-ordered phase is characterized by a finite value of the order parameter

$$O_{\rm BO} = \frac{1}{L}\sum_i (-1)^i B_i, \tag{11}$$

where $B_i = \langle a_i^\dagger a_{i+1} + a_{i+1}^\dagger a_i\rangle$. Dimer-dimer correlator $\langle B_i B_{i+r}\rangle$ behaves as $\propto e^{-r/\xi}$ capturing a length scale ξ in the gapped regime. Transition to the gapless scale is characterized by $\xi \to \infty$. Since the $\phi = \pi$ BO phase has a finite excitation gap, we expect it to be stable for the small deviation of ϕ from π. DMRG results are plotted in Fig. 8 where we show both the BO order parameter as well as the two-point correlation function for the bond order near $\phi = \pi$. One finds an extended BO phase where the lobe of BO order is roughly centered about $t_2/t_1 = -0.5$ which is the Majumdar-Ghosh point [68,70,71] for which the the BO ground state is exact at $\phi = \pi$. The structure of the lobe shows that at a fixed $0.79\pi \lesssim \phi < \pi$ there is a reentrant transition into a $c = 1$ TLL as we tune t_2/t_1 from positive to negative. At $t_2/t_1 = -\infty$ we have two decoupled chains which are in a separate TLL phase. Turning on a positive t_1 destroys this state in favor of a bond order. However, we note that our calculations suggest that turning on a ϕ away from

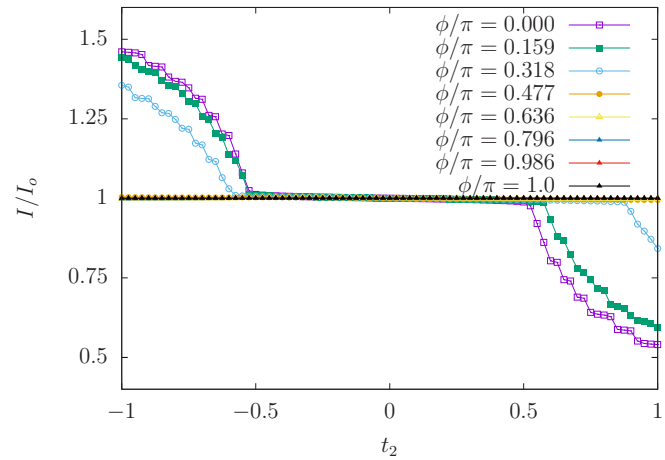

FIG. 7. Moment of inertia: Variation of $I = \int dk \langle n(k)\rangle (\sin(k))^2$ with t_2 for different values of ϕ. I_o is the corresponding value for a half-filled Fermi sea at $t_2 = 0$ ($L = 62$).

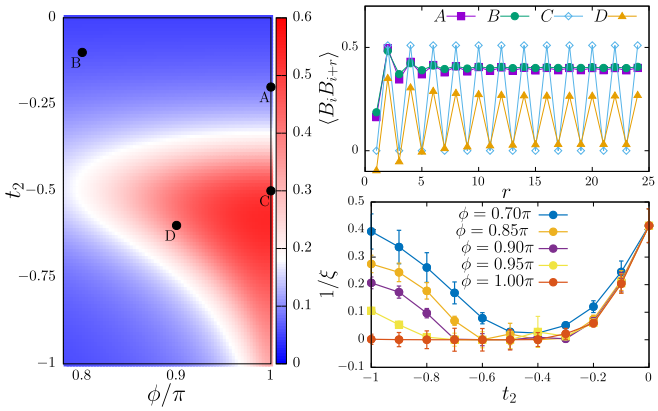

FIG. 8. Bond-ordered phase: (Left) $|O_{\rm BO}|$ as a function of ϕ and t_2 in the gapped regime. (Top right) Dimer-dimer correlator $\langle B_i B_{i+r}\rangle$ and its behavior as a function of r is shown at the marked points (A–D) on the left. (Bottom right) Fitting $\langle B_i B_{i+r}\rangle \propto e^{-r/\xi}$; behavior of $1/\xi$ with t_2 for different values of ϕ.

$\phi = \pi$ instead favors an instability to a $c = 1$ TLL which competes with BO leading to a domelike structure.

3. *Phase boundaries and the phase transitions*

Our discussion up to now has described the two metallic phases and the gapped phase. We now describe the phase boundaries and their characterization via DMRG. There are two types of phase boundaries denoting quantum phase transition between (1) $c = 1$ TLL [equivalently a power-law superfluid (SF)] to the symmetry broken bond-ordered phase, and (2) $c = 1$ and $c = 2$ TLL phases.

Fidelity: To analyze the phase boundaries, one particularly useful quantity to examine is the ground state fidelity. Given two ground state wave functions evaluated at parameters λ and $\lambda + d\lambda$, the fidelity susceptibility is given by [72]

$$\chi_F(\lambda) = \lim_{d\lambda\to 0} \frac{-2\log[|\langle\psi(\lambda + d\lambda)|\psi(\lambda)\rangle|]}{(d\lambda)^2}. \qquad (12)$$

Signatures in χ_F signal phase transitions. Figure 9 shows the behavior of χ_F while going from gapless to gapped regime [Figs. 9(a) and 9(b)] and between gapless to gapless regime [Figs. 9(c) and 9(d)] for different system sizes. Note that χ_F behaves rather differently at the two kinds of transition. In order to corroborate our DMRG results we compare the results for small system sizes with exact diagonalization (ED) studies. Some representative results are shown in Fig. 10.

Central charge and gap: While the Lifshitz transition between the two TLLs is characterized by a sudden jump in central charge c, the boundary between the gapped phase and $c = 1$ TLL shows a smooth transition with systematic finite size scaling (see Appendix D).

To estimate the phase boundaries we use the excitation gap Δ_L [see Eq. (9)]. Behavior of Δ_L as a function of t_2 across the gapless-gapless transition is rather abrupt. A few representative plots for $\phi/\pi = 0.28$ and $\phi/\pi = 0.42$ for three different values of $L = 200, 240, 300$ is shown in Fig. 11. We now analyze the transition between the gapped and gapless phase near $\phi = \pi$. At $\phi = \pi$ the transition has been shown to be BKT like [68]. During such a transition it is useful to

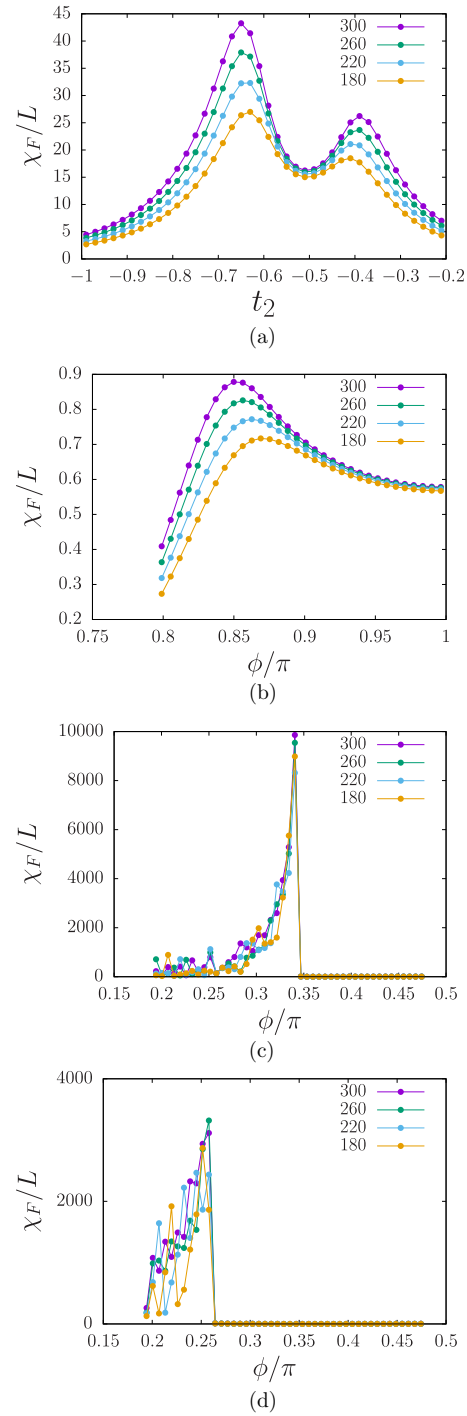

FIG. 9. Fidelity susceptibility χ_F: (a) as a function of t_2 at $\frac{\phi}{\pi} = 0.8732$ and (b)–(d) as a function of ϕ/π for $t_2 = -0.46$, 1.00, and 0.7. The humps signal phase transitions.

analyze the variation of $\Delta_L L$ with $\log L - \frac{a}{\sqrt{V - V_c}}$, where V is any tuning parameter and V_c is the critical value [73,74]. Defining $x_L = \log L - \frac{a}{\sqrt{V - V_c}}$, values of $\Delta_L L$ and corresponding x_L for various L and V near V_c (in the gapped regime) can be fitted to a curve. Treating a and V_c as variational parameters, the least square fitting error is minimized to optimize a, V_c (see Fig. 11). We use this data collapse to determine the gapless-gapped transition boundary as shown in Fig. 2.

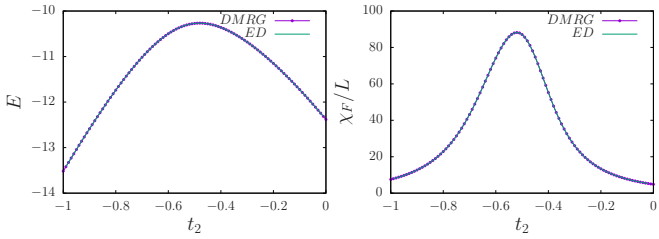

FIG. 10. DMRG and ED: Ground state energy and fidelity susceptibility χ_F/L as a function of t_2 for $\phi/\pi = 0.859$ for a system size $L = 20$ under open-boundary condition, both using exact diagonalization and DMRG.

IV. BOSONIZATION: THE PHASES AND PHASE TRANSITIONS

The fluctuation about the HF theory can be systematically taken into account in one dimension using the framework of Abelian bosonization to understand both the phases as well as the phase transitions out of the metallic states. As an immediate well-known fallout of the fluctuations, the quasiparticles in the metals are no longer well defined resulting in TLLs which are one-dimensional non-Fermi liquid metals. In the regime $t_2/t_1 < 0.5$, the Hartree-Fock treatment (Sec. III A) as discussed above leads to a dispersion as schematically shown in Fig. 3(a). In general this *free* theory has two Fermi points (k_F^L and k_F^R) centered about $k_o \neq 0$ and the Fermi velocities (v_f^R and v_f^L) are different. Further Luttinger theorem restricts $k_F^R - k_F^L = \pi$ at half-filling. The low energy excitations about the HF ground state constitute single particle excitations about these two Fermi points which can be understood within a low energy linearized (about the left and the right Fermi points) theory about the HF ground state given by

$$\mathcal{H}_0 = -\mathbb{i} \int dx \big[v_f^R \Psi_R^\dagger \partial_x \Psi_R - v_f^L \Psi_L^\dagger \partial_x \Psi_L \big], \tag{13}$$

where (Ψ_R, Ψ_L) are left and right moving fermions and in the present case for $\phi, t_2 \neq 0$ the corresponding Fermi velocities. A standard bosonization treatment [75] in terms of the bosonic fields $\Theta(x,t)$ and $\Phi(x,t)$ satisfying

$$[\nabla\Phi(x), \Theta(y)] = [\nabla\Theta(x), \Phi(y)] = i\pi\delta(x-y) \tag{14}$$

leads to the following free theory linearized about the HF ground state

$$\tilde{\mathcal{H}}_0 = \frac{V_F}{2\pi} \int dx[(\partial_x\Phi)^2 + (\partial_x\Theta)^2] + \frac{W}{2\pi} \int dx[\partial_x\Phi\partial_x\Theta + \partial_x\Theta\partial_x\Phi], \tag{15}$$

where $V_F = \frac{v_f^R + v_f^L}{2}$ and $W = \frac{v_f^R - v_f^L}{2}$. As discussed in Appendix E, the interaction term for the bosonized modes is given by (where the normal ordering is done about the HF ground state)

$$H_{\rm int} = \tilde{H}_{\rm int}^{\rm Fow} + \tilde{H}_{\rm int}^{\rm Ump}, \tag{16}$$

where

$$\tilde{H}_{\rm int}^{\rm Fow} = V \int dx[(\partial_x\Phi)^2 - (\partial_x\Theta)^2], \tag{17}$$

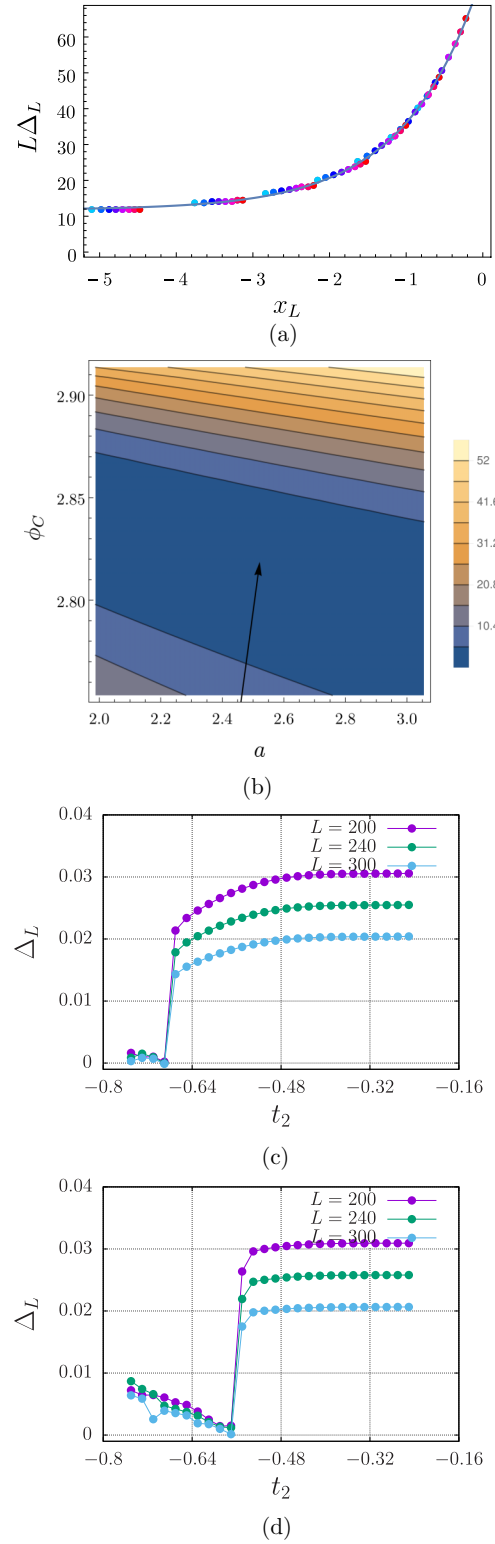

FIG. 11. Excitation gap at phase transitions: (a) and (b) Best obtained collapse of $\Delta_L L$ and $x_L = \log L - \frac{a}{\sqrt{\phi-\phi_c}}$ by variation of a, ϕ_c. The estimation of a, ϕ_c is done by minimizing the fitting error. Here, this is done for the transition from gapless to gapped point as a function of ϕ for $t_2 = -0.70$. (c) and (d) Behavior of Δ_L as a function of t_2 across the gapless-gapless transition for $\phi/\pi = 0.28$ and $\phi/\pi = 0.42$ for three different values of $L = 200, 240, 300$. Notice that unlike the gapless-gapped transition, for any finite L, Δ_L shows a jump to zero at the Lifshitz transition.

where $V = 4t_2[\cos(\phi + 2k_o) - \cos(2k_o)]$ denotes the forward scattering among the low energy left and right moving fermions, and

$$\tilde{H}_{\text{int}}^{\text{Ump}} = -\lambda \int dx \cos 4\Phi, \tag{18}$$

with $\lambda = -2V$. Gathering all the terms we get the bosonized Hamiltonian to be

$$H = \frac{v_f}{2\pi} \int dx \left[\frac{1}{K} (\partial_x \Phi)^2 + K (\partial_x \Theta)^2 \right] - \frac{W}{2\pi} \int dx [\partial_x \Phi \partial_x \Theta + \partial_x \Theta \partial_x \Phi] - \lambda \int dx \cos 4\Phi, \tag{19}$$

where the renormalized average Fermi velocity is given by $v_f = \sqrt{(V_F)^2 - 4\pi^2 V^2}$ and the Luttinger parameter is given by

$$K = \sqrt{\frac{V_F - 2\pi V}{V_F + 2\pi V}}. \tag{20}$$

From the expression it is clear, as expected, V and λ both go to zero at $\phi = 0$ and hence at this point, $K = 1$. Also, as expected, $W = 0$ in this limit. This is nothing but the free fermions. Thus, while V kills the quasiparticles by renormalizing the Luttinger parameter K, λ destabilizes the TLL leading to bond order.

To understand the effect of the other terms, we derive the corresponding real time action which is given by

$$\mathcal{S} = \frac{1}{2\pi v_f K} \int dt dx \left[\left(\partial_t \Phi + \frac{w}{2} \partial_x \Phi \right)^2 - v_f^2 (\partial_x \Phi)^2 \right] + \lambda \int dt\, dx \cos 4\Phi, \tag{21}$$

where $w = W/\Delta\tau$ where the limit is taken such that w is constant. The effect of the "boost" can then be "gauged away" [76] after which we can wick rotate it to imaginary time to get the Euclidean action

$$\mathcal{S}_E = \frac{1}{2\pi v_f K} \int d\tau dx \left[(\partial_\tau \Phi)^2 + v_f^2 (\partial_x \Phi)^2 \right] - \lambda \int d\tau\, dx \cos 4\Phi. \tag{22}$$

We use the relation between Luttinger parameter K and the fermion two-point correlator

$$C(r) := \frac{1}{L} \sum_i \langle c_i^\dagger c_{i+r} \rangle \sim \frac{1}{r^{(K+1/K)/2}} \tag{23}$$

to extract K from DMRG results and compare them with the values obtained from the bosonized theory. Away from the gapped region, where the Umklapp processes are small, the bosonization result compares well with DMRG results as seen in Fig. 12. For a fixed t_2, the Umklapp amplitude λ increases monotonically with ϕ such that the Umklapp scattering becomes important ultimately making the TLL unstable to a gapped BO phase. In the latter case, the bosonization values of K, λ should be viewed as initial points of the RG flow as shown in Fig. 12. The instability to a gapped phase is also

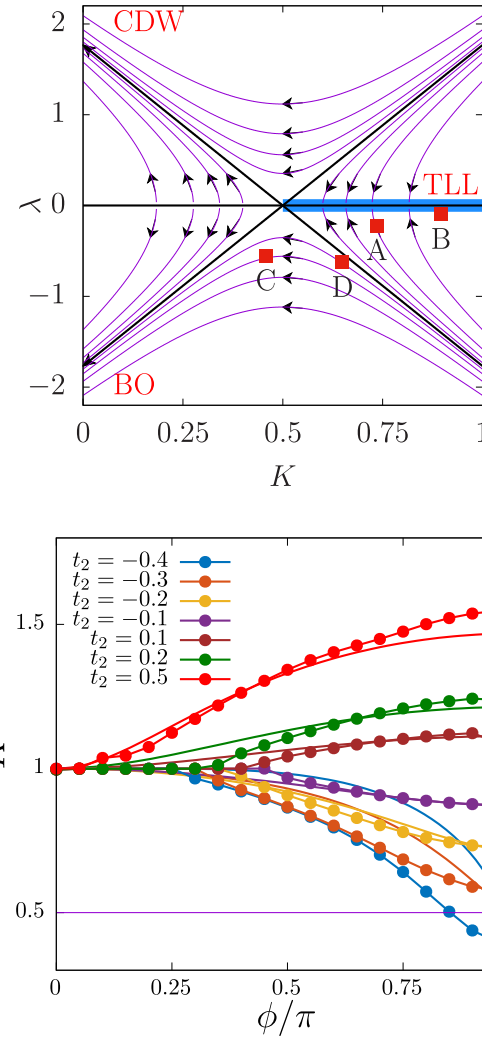

FIG. 12. Bosonization and BKT transition: (Top) Luttinger parameter (K) and λ calculated from the bosonization result for a set of parameters of $\{t_2, \phi/\pi\}$ as shown by (A–D) in Fig. 8 [see near Eq. (19)] are shown by square points on the RG flow diagram of the BKT transition with TLL, BO, and charge density wave (CDW) phases. V and λ are scaled by multiplicative prefactors of $\alpha/2\pi$ and α, respectively, where $\alpha \approx 0.3$. (Bottom) A plot of numerically extracted K from the DMRG using $\langle c_i^\dagger c_{i+r} \rangle$ correlators and compared with the bosonization result.

manifested through the Luttinger parameter reaching a critical value of $K = 1/2$ as anticipated from a perturbative RG calculation. Away from the bond-ordered phase, for generic values of $2K > 1$ our numerical calculation suggest a direct transition between the present TLL with central charge $c = 1$ to another with central charge $c = 2$.

While a similar construction can be obtained for the $c = 2$ TLL by linearizing about the four Fermi points and introducing two pairs of left and right moving fermions, characterizing this low energy theory requires characterizing the 2×2 *matrix Luttinger parameter* [77], which we do not pursue here in detail except to understand the critical point between the $c = 1$ and $c = 2$ TLLS (see below).

Therefore, starting with the above $c = 1$ TLL, we now try to understand the entire phase diagram including the phase

transition between the $c = 1$ TLL and the BO phase as well as between the $c = 1$ and $c = 2$ TLLs.

A. Transition between the power-law SF to BO phase

Our numerical calculations show that the entire phase boundary is captured by a BKT type phase transition. This is expected in the $\phi = \pi$ limit, where we have hard-core bosons and an application of XY duality in $(1 + 1)D$ [78] captures both the SF and the BO phases where extra Berry phases induce breaking of inversion symmetry in the BO phase [79].

To understand this transition to general ϕ, it is convenient to use the bosonized field theory by writing down the Euclidean action in Eq. (21). The effect of finite ϕ is to provide a "boosted" field theory where the effect of the "boost" can then be gauged away [76]. The Umklapp scattering then drives the BO instability gapping out the TLL as can be seen in the behavior of the Luttinger parameter (see Fig. 12). The corresponding RG flows based on the Sine-Gordon theory (Fig. 12) effectively capture the phase transition along with the phases.

B. Transition between $c = 1$ and $c = 2$ TLL

Within HF, the gapless-gapless transition is a Lifshitz transition [see schematic Fig. 3(b)]. Our central charge calculations from DMRG suggest that the Lifshitz transition for finite ϕ from $c = 1$ CFT (TLL with two Fermi points) to $c = 2$ CFT (TLL with four Fermi points) is a sudden one when compared to the BKT transition. However, crucially there is no local real space order parameter based description for this quantum phase transition which then requires careful examination regarding its nature. The HF band structure suggests that the low energy modes near this transition contains the linearly dispersing left ψ_L and right ψ_R fermions along with quadratically dispersing holes of the central lobe ψ_c (see Fig. 3).

At $\phi = 0$, these modes are noninteracting and hence the HF theory is exact and the transition at $t_2/t_1 = -0.5$ is given by a dynamical exponent $z = 2$ theory where changing t_2 has the primary effect of changing the hole chemical potential leading to finite density of holes. For $\phi \neq 0$, even within HF theory the there is renormalization of the Fermi velocities of both ψ_L and ψ_R, but these modes do not couple to ψ_c. Assuming that the above three-mode picture holds for at least finite but small $\phi \neq 0$, we now can add fluctuations within the bosonization framework where we bosonize the left and right fermions to get the following effective low energy Hamiltonian $\mathcal{H} = H + H'$, where where H is given by Eq. (19) and

$$H' = \int dx\, \psi_c^\dagger \left[\frac{\partial_x^2}{2m^*} - \mu\right]\psi_c + \int dx (g_1 \partial_x \Phi + g_2 \partial_x \Theta)\psi_c^\dagger \psi_c. \tag{24}$$

The first term in H' is the free action of the quadratically dispersing fermionic holes with effective mass m^* and chemical potential μ which is zero at $t_2/t_1 = -0.5$ and increases (decreases) for $t_2/t_1 < -0.5$ (> -0.5) and thereby capturing the HF phase transition. The advantage of this formulation is by bosonizing the left and right fermions we have been able to take into account their mutual interactions through the forward scattering channel by renormalizing the Luttinger parameter and the Fermi velocity as before. g_1 and g_2 are two symmetry allowed coupling constants, which are given in terms of the microscopic parameters as

$$g_1 = -4t_2[\{\cos(\phi + 2k_c) - \cos(2k_c)\} - \{\cos(\phi + 2k_o) - \cos(2k_o)\}], \tag{25}$$

$$g_2 = -8t_2[\sin(k_o + k_c + \phi) - \sin(k_o + k_c)]. \tag{26}$$

Note that near $\phi = 0$, $g_1 \sim -8t_2\phi\{k_o - k_c\}$ and $g_2 \sim -8t_2\phi$ and $|(k_o - k_c)| \propto t_2\phi$. Hence, at $\phi = 0$, as is expected, $k_o = k_c = 0$ and $g_1 = g_2 = 0$ leading to the free fermionic description. Also, the microscopic symmetry of combination of parity ($\mathcal{P}$) and time reversal ($\mathcal{T}$) together, remains intact in this description ($\mathcal{P} : \Phi \to -\Phi, \Theta \to \Theta$ and $\mathcal{T} : \Phi \to \Phi, \Theta \to -\Theta$).

The effective Euclidean action is

$$\mathcal{S} = \frac{1}{2v_f K\pi}\int dx d\tau \left\{\left[\dot{\Phi} - i\frac{W}{2}\partial_x\Phi + ig_2\pi\psi_c^\dagger(x)\psi_c(x)\right]^2 + v_f^2(\partial_x\Phi)^2\right\} + g_1\int dx d\tau[\psi_c^\dagger(x)\psi_c(x)\partial_x\Phi] + \int dx\psi_c^\dagger\left[\frac{\partial_x^2}{2m^*} - \mu\right]\psi_c - \lambda\int dx d\tau\cos(4\Phi). \tag{27}$$

Redefining a boosted field such that $\dot{\Phi} \equiv \dot{\Phi} - i\frac{W}{2}\partial_x\Phi$, $\partial_x\Phi = \partial_x\Phi$,

$$\mathcal{S} = \frac{1}{2v_f K\pi}\int dx d\tau\left\{[\dot{\Phi} + ig_2\pi\Psi_c^\dagger(x)\Psi_c(x)]^2 + v_f^2(\partial_x\Phi)^2\right\} + g_1\int dx d\tau[\Psi_c^\dagger(x)\Psi_c(x)\partial_x\Phi] + \int dx\psi_c^\dagger\left[\frac{\partial_x^2}{2m^*} - \mu\right]\psi_c - \lambda\int dx d\tau\cos(4\Phi). \tag{28}$$

In Fourier space the above action becomes

$$\mathcal{S} = \mathcal{S}_\Phi + \mathcal{S}_c + \mathcal{S}_{\rm int}, \tag{29}$$

where

$$\mathcal{S}_\Phi = \frac{1}{2\pi v_f K}\int dq\, d\omega\left[\omega^2 + v_f^2 q^2\right]|\Phi(q,\omega)|^2, \tag{30}$$

$$\mathcal{S}_c = \int dq\, d\omega\left[i\omega + \left(\frac{k^2}{2m^*} - \mu\right)\right]\psi_c^\dagger(k,\omega)\psi_c(-k,-\omega), \tag{31}$$

$$\mathcal{S}_{\rm int} = ig\int d\omega_1 dq_1 d\omega_2 dq_2\,[i\omega_1 - \alpha q_1] \times \Phi(q_1,\omega_1)\psi_c^\dagger(q_2,\omega_2)\psi_c(q_1+q_2,\omega_1+\omega_2), \tag{32}$$

where $g = g_2/(v_f K)$ and $\alpha = g_1 v_f K/g_2$. Similar field theories are suggested in the context of multimode wires [56,80,81].

The short range four fermion term for the central mode (ψ_c) are irrelevant at this critical point which is understandable due to the paucity of the phase space for such density-density scatterings.

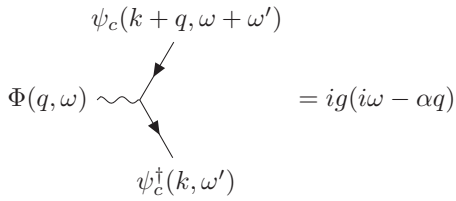

FIG. 13. Scattering vertex: The scattering vertex between the bosonized modes and the central fermions when the HF solution shows a Lifshitz transition.

The scattering vertex between the bosonized modes and the central fermions is shown in Fig. 13. Also, the chemical potential is always a relevant perturbation for the ψ_c fermions at the $\mu = 0$ fixed point.

Perturbative one-loop RG calculations around the $\mu = g_1 = g_2 = 0$ yields the β function for the Luttinger parameter

$$\frac{dK}{dl} = C\mu\left[\left(\frac{g_1 K}{g_2}\right)^2 - 1\right], \tag{33}$$

where $C \propto \frac{g_2^2}{2v_f}$. We find that near $\phi \to 0$ this term does not lead to a run-away flow signaling a stable phase within this approximation. However, a full characterization requires further studies. Remarkably just tuning the statistical phase of pseudofermions can mediate this transition between two non-Fermi liquids neither of which has low energy quasiparticles.

V. SUMMARY AND OUTLOOK

To summarize, we have shown that a simple quadratic system of pseudofermions hopping on 1D lattice with nearest- and next-nearest-neighbor hopping following fractionalized algebra [Eq. (1)], has a rich phase diagram with gapless TLL phases and gapped BO phases which can be accessed by solely tuning the *statistical parameter*. The tunability of statistics can be accomplished in two ways: pseudobosons and pseudofermions. While the former has an infinite Hilbert space per site and requires strong on-site repulsion to have hard-core constraint, in the latter such hard-core exclusion is natural. Our study has illustrated the rich physics behind a simple pseudofermionic model and hence provides a new direction to further explore the intervening phases and phase transitions between many body phases which are otherwise understood for fermions and spin models.

An alternate view point closer to the context of solid-state materials is that the above pseudofermion hopping model is equivalent to a correlated hopping problem, where owing to interactions, the single particle *kinetic energy* can be quenched leading to correlated motion. It is known that in two dimensions such constrained kinetic energy can lead to novel phases such as integer quantum Hall effect of hard-core bosons [65] as well as superconductivity [50,51,62,63]. The rich phase diagram arising out of our calculations then makes the above model a minimal starting point to understand a host of interesting questions in correlated quantum many-body systems in one dimension. In particular, apart from the BKT phase transition, the possibility of a continuous Lifshitz transition between two TLLs with central charges $c = 1$ and 2 is extremely interesting. While normally Lifshitz transition in Fermi liquids allows for a nominal quasiparticle description, we note that in the present case, once fluctuations are taken into account over the HF theory, there are no quasiparticles at lowest energies. Thus this serves as an example of an unconventional quantum phase transition between two robust metallic phases (devoid of quasiparticle excitations) that cannot be captured within an order-parameter based Landau-Ginzburg theory.

At this point we would like to emphasise that both the transitions can be engendered by solely tuning the statistical angle ϕ. Moreover, while the BO phase disappears away from half-filling due to the absence of Umpklapp scattering, the Lifshitz transition is robust. Furthermore, the effect of third (or higher) neighbor hopping terms are expected to be irrelevant showing that these phases and phase transitions are not fine-tuned points, but rather robust and expected to be generically present in *pseudofermionic* phase transitions.

While the model we have discussed does not pertain to a particular experimental setup at present, some of the recent proposals [13,82,83] of generating off-site correlated hopping in fermionic ultracold atoms are extremely promising. In particular the recent experimental realizations of the Creutz ladder [47] and the chiral ladder [48] comprises of an interesting setup where the effective 'Wannier orbitals" of the potential wells of an optical lattice act as on-site orbitals which are further coupled via resonantly tuned lasers to produce tunable hopping strengths. This setup can be effectively converted to a our setup of a zigzag ladder (see Fig. 1) by introducing a tilt in one of the directions thereby increasing the intersite hopping strength. The intensity of tilt could be potentially used to modulate the hopping parameters to access the Lifshitz transitions which will correspond to the $\phi = 0$ limit of our phase diagram (see Fig. 2). A recent proposal to introduce correlated hoppings, albeit presently realized in a ^{40}K setup [38], can also be promising. Finally, the connection of the present model and its relevance to understand the edge physics of both quantum Hall ribbons, particularly in context of recent advancements with experiments on synthetic Hall ribbons [44], forms promising future directions.

ACKNOWLEDGMENTS

We acknowledge fruitful discussions with Diptiman Sen, H. R. Krishnamurthy, Krishnendu Sengupta, Subroto Mukerjee, Smitha Vishveshwara, R. Loganayagam, Avinash Dhar, R. Moessner, Tapan Mishra, Arun Parmakanti, and Sumilan Banerjee. A.A. and S.B. acknowledges MPG for funding through the Max Planck Partner group on strongly correlated systems at ICTS. S.B. acknowledges SERB-DST (India) for funding through project Grant No. ECR/2017/000504. V.B.S. acknowledges support from DST (India). DMRG calculations are performed using ITensor [66]. The numerical calculations were done on the cluster *Mowgli*, *boson*, and *zero* at the ICTS and *Sahastra* at IISc. We acknowledge ICTS and the discussion meeting "New questions in quantum field theory from condensed matter theory" during which some of these ideas originated.

APPENDIX A: DETAILS OF THE SYMMETRIES OF THE MICROSCOPIC HAMILTONIAN

The one-dimensional chain with nearest- and next-nearest-neighbor coupling can be alternatively thought of as a zigzag ladder (Fig. 1) with the following symmetries at generic values of ϕ:

(1) Lattice translation by unit lattice spacing of the one dimensional chain T_x.

(2) Combination of time-reversal ($\mathcal{T}$) and parity ($\mathcal{P}$) as $\mathcal{Q} = \mathcal{P}\mathcal{T}$.

Under T_x, the fermions transform as

$$T_1 c_i {T_1}^{-1} = c_{i+1} \quad T_{-1} c_i {T_{-1}}^{-1} = c_{i-1},$$
$$T_1 c_L {T_1}^{-1} = c_1, \quad T_{-1} c_1 {T_{-1}}^{-1} = c_L. \tag{A1}$$

Note that we have we have L sites labeled $\{1 \cdots L\}$ where L is taken to be an even number. Thus on the pseudofermions a_i, translations act as

$$T_1 a_i {T_1}^{-1} = T_1 K_i^\dagger c_i {T_1}^{-1} = e^{-i\phi n_1} K_{i+1}^\dagger c_{i+1} = e^{-i\phi N_1} a_{i+1},$$
$$T_{-1} a_i {T_{-1}}^{-1} = T_{-1} K_i^\dagger c_i {T_{-1}}^{-1} = e^{i\phi n_L} K_{i-1}^\dagger c_{i-1} = e^{i\phi N_L} a_{i-1}. \tag{A2}$$

Similarly, under $\mathcal{T}$ and $\mathcal{P}$, the fermion operators transform in the following way:

$$\mathcal{T} c_i \mathcal{T}^{-1} = c_i, \quad \mathcal{T} c_i^\dagger \mathcal{T}^{-1} = c_i^\dagger, \tag{A3}$$

$$\mathcal{P} c_i \mathcal{P}^{-1} = c_{L-i+1}, \quad \mathcal{P} c_i^\dagger \mathcal{P}^{-1} = c_{L-i+1}^\dagger. \tag{A4}$$

This results in the following transformation for the pseudofermion operators a_i:

$$\mathcal{T} a_i \mathcal{T}^{-1} = \mathcal{T} K_i^\dagger c_i \mathcal{T}^{-1} = K_i c_i,$$
$$\mathcal{P} a_i \mathcal{P}^{-1} = \mathcal{P} K_i^\dagger c_i \mathcal{P}^{-1} \tag{A5}$$
$$= e^{i\phi\mathcal{N}} K_{L-i+2} c_{L-i+1} = e^{i\phi\mathcal{N}} K_{L-i+1} c_{L-i+1}, \tag{A6}$$

where $\mathcal{N} = \sum_i N_i = \sum_i n_i$. Thus, under the combination of these symmetries $\mathcal{Q}$, the a_i transform as

$$\mathcal{Q} a_i \mathcal{Q}^{-1} = e^{-i\phi\mathcal{N}} a_{L-i+1},$$
$$\mathcal{Q} a_i^\dagger \mathcal{Q}^{-1} = a_{L-i+1}^\dagger e^{i\phi\mathcal{N}}. \tag{A7}$$

APPENDIX B: FREE FERMIONIC LIMIT: BAND STRUCTURES, FERMI VELOCITY, AND FERMI POINTS

1. Band structures

The free fermion dispersion at any value of t_2 is given by

$$E(k) = -2t_1 \cos k - 2t_2 \cos 2k. \tag{B1}$$

The dispersions for few representative values of t_2 (keeping $t_1 = 1$) are shown in Fig. 14.

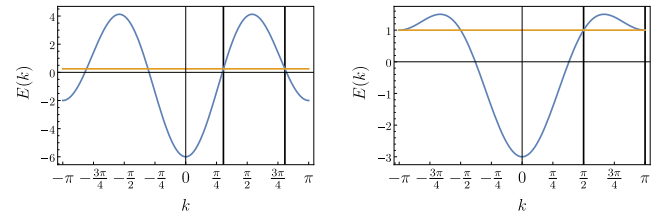

(a)Dispersion when $\phi = 0$ and $t_2 = 2$ (b)Dispersion when $\phi = 0$ and $t_2 = 0.5$

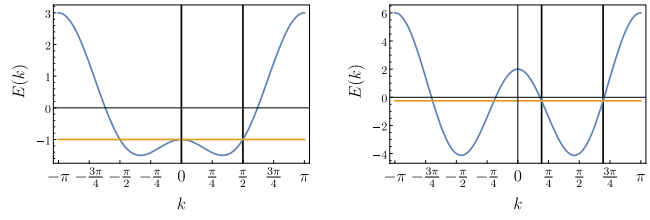

(c)Dispersion when $\phi = 0$ and $t_2 = -0.5$ (d)Dispersion when $\phi = 0$ and $t_2 = -2$

FIG. 14. Free fermion limit: Single particle dispersion for the fermion problem in $\phi = 0$ limit (we have set $t_1 = 1$ throughout). For $t_2 > 0$ depending on the value of t_2 we can either have two (for $|t_2| < \frac{1}{2}$) Fermi points (at $\pm\pi/2$) or four (for $|t_2| > \frac{1}{2}$) Fermi points. The Fermi level corresponds to that for half-filling. Note that the system undergoes a Lifshitz transition as a function of t_2/t_1.

2. Fermi points

At 1/2-filling, for $-1/2 < t_2 < 1/2$, there are two Fermi points at $k = \pm\pi/2$. For $|t_2| > 1/2$, there are four Fermi points $(k_F^{R\pm}, k_F^{L^\pm})$ given by

$$\text{For } t_2 > 1/2: \begin{cases} k_F^{R+} = \arccos\left(\frac{-1}{2\sqrt{2}t_2}\right) - \frac{\pi}{4}, \\ k_F^{L+} = k_F^{R+} + \frac{\pi}{2}, \\ k_F^{R-} = -k_F^{L+}, \\ k_F^{L-} = -k_F^{R+}, \end{cases} \tag{B2}$$

$$\text{For } t_2 < 1/2: \begin{cases} k_F^{R+} = \arccos\left(\frac{1}{2\sqrt{2}|t_2|}\right) + \frac{\pi}{4}, \\ k_F^{L+} = k_F^{R+} - \frac{\pi}{2}, \\ k_F^{R-} = -k_F^{L+}, \\ k_F^{L-} = -k_F^{R+}. \end{cases} \tag{B3}$$

Therefore at $\phi = 0$, as a function of t_2, we have Lifshitz transition for finite filling.

3. Fermi velocity

The Fermi velocity can be determined by the slope of the dispersing band at the Fermi points. For $|t_2| < \frac{1}{2}$ the Fermi points remain pinned at $k_F = \pm\frac{\pi}{2}$ at half-filling due to Luttinger theorem and the corresponding Fermi velocities continue to be

$$v_F = \left.\frac{\partial E(k)}{\partial k}\right|_{k=k_F} = \pm 2t_1. \tag{B4}$$

For $|t_2| > \frac{1}{2}$ the Fermi velocities at the four Fermi points depend on t_2 and are given by

$$\left(2t_1 \sin k_F^{R/L\pm} + 4t_2 \sin 2k_F^{R/L\pm}\right), \tag{B5}$$

respectively.

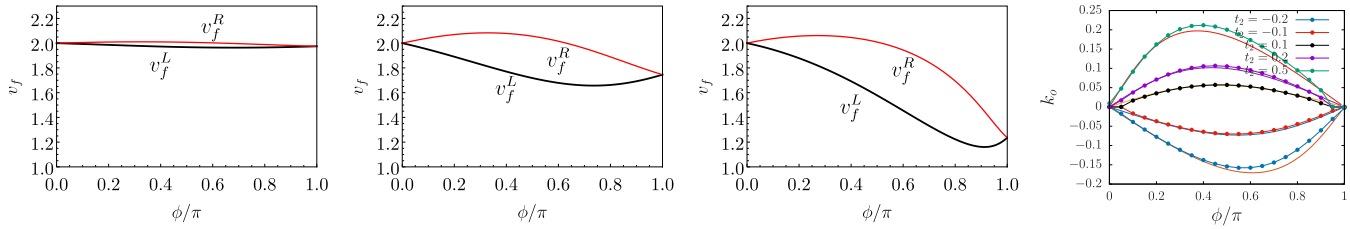

FIG. 15. Fermi velocities: The right and left Fermi velocities (v_f^R and v_f^L) as a function of ϕ for $t_2 = -0.01$, $t_2 = -0.1$, and $t_2 = -0.3$. Notice that the right and left velocities are different. The rightmost figure shows the comparison of shifted center of the Fermi sea $\equiv k_o$ from both HF and the DMRG study for various values of t_2 and as a function of ϕ.

APPENDIX C: HARTREE-FOCK THEORY

The Hartree-Fock decomposition of the interactions in Eq. (8) is obtained as

$$c^\dagger_{k_1} c^\dagger_{k_2} c_{k_3} c_{k_4} \to -\langle c^\dagger_{k_1} c_{k_3}\rangle c^\dagger_{k_2} c_{k_4} - c^\dagger_{k_1} c_{k_3}\langle c^\dagger_{k_2} c_{k_4}\rangle + \langle c^\dagger_{k_1} c_{k_4}\rangle c^\dagger_{k_2} c_{k_3} + c^\dagger_{k_1} c_{k_4}\langle c^\dagger_{k_2} c_{k_3}\rangle. \quad \text{(C1)}$$

Keeping only the density mode $\langle n_k\rangle = \langle c^\dagger_k c_k\rangle$ gives us the Hartree-Fock Hamiltonian

$$H_{\rm HF} = \sum_k \{\varepsilon_0(k) + A(k) + B + C(k)\} c^\dagger_k c_k, \quad \text{(C2)}$$

where

$$A(k) = 2t_2 \sum_{k'} \{(e^{i\phi} - 1) e^{i(k+k')} + \text{H.c.}\}\langle n(k')\rangle, \quad \text{(C3)}$$

$$B = -2t_2 \sum_{k'} \{\cos(\phi + 2k') - \cos(2k')\}\langle n(k')\rangle, \quad \text{(C4)}$$

$$C(k) = -2t_2 \left\{\sum_{k'} \langle n(k')\rangle\right\} \{\cos(\phi + 2k) - \cos(2k)\}. \quad \text{(C5)}$$

Solving this self-consistently for $\langle n(k)\rangle = \langle c^\dagger_k c_k\rangle$ produces the renormalized single particle dispersion for different values of the parameters.

The Hartree-Fock dispersion as a function of $\{t_2, \phi\}$ shows Lifshitz transitions which closely follow the phase transition between the $c = 1$ and $c = 2$ TLLs (see Fig. 2).

In the $c = 1$ phase, HF calculation illustrates that the center of the Fermi sea is shifted and the occupied states have momenta $k_o - \frac{\pi}{2} \leqslant k \leqslant k_o + \frac{\pi}{2}$ where the shift of the center k_o is given by

$$\sin(k_o) = \frac{4t_2}{\pi} \sin\left(\frac{\phi}{2}\right) \cos\left(\frac{\phi}{2} + 2k_o\right). \quad \text{(C6)}$$

In this phase the HF Hamiltonian can be linearized about the two Fermi points by introducing the left and right moving fermion fields Ψ_L and Ψ_R, respectively, to get the linearized Hamiltonian in real space as given in Eq. (13). Due to breaking of the time-reversal symmetry for general ϕ, the Fermi sea center gets shifted from $k = 0$ ($\equiv k_o$) and the two Fermi velocities at the Fermi points can in general be different. The variation of Fermi velocities and k_o as a function of few parameters is shown in Fig. 15.

APPENDIX D: ENTANGLEMENT ENTROPY AND CENTRAL CHARGE

In DMRG we work with open-boundary condition—here it is known from the Cardy-Calabrese formula that entanglement entropy of a subsystem size l as a function of l/L can be fitted to the following form [67]:

$$S(l) = \frac{c}{6} \ln\left[\frac{L}{\pi} \sin\left(\frac{\pi l}{L}\right)\right] + \cdots \quad \text{(D1)}$$

to estimate c, the central charge.

Behavior of central charge across the BKT transition is shown in Fig. 16 for a few parameters where central charge changes from 1 to zero where the same for the gapless-gapless transitions are shown in Fig. 17. Note the abrupt change in c in contrast to the smooth variation in c for the gapless-gapped transition.

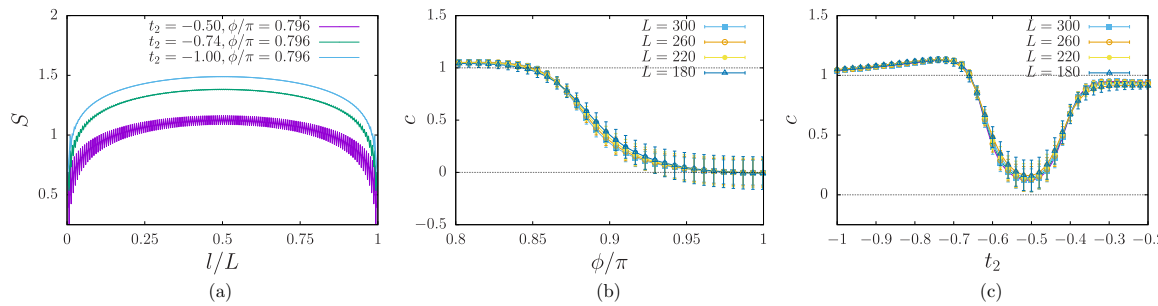

FIG. 16. Entanglement entropy and central charge: (a) Entanglement entropy for three different parameters of t_2, ϕ as a function of bond length l/L for $L = 300$. The central charge (c) is estimated using the Cardy-Calabrese formula. Variation of c for four different system sizes as a function of ϕ for $t_2 = -0.60$ (b) and as a function of t_2 for $\phi/\pi = 0.891$ (c).

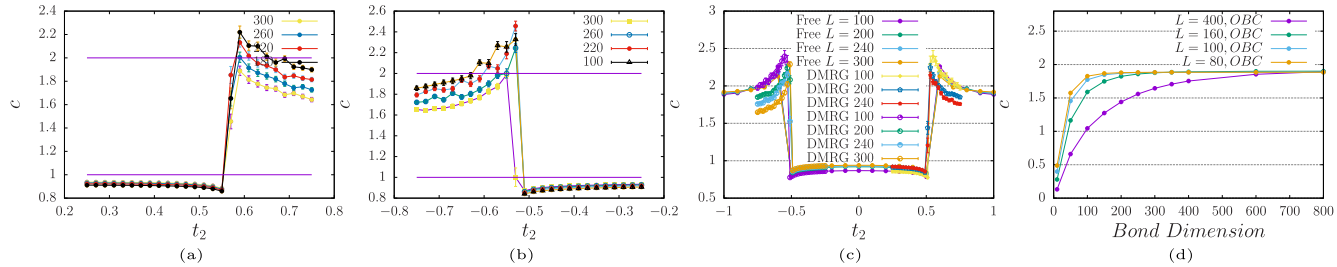

FIG. 17. Transition in central charge: The variation of central charge c as a function of t_2 for $\phi/\pi = 0.159$ (a) and $\phi/\pi = 0.18$ (b) showing a gapless-gapless transition between the $c = 1$ and $c = 2$ phases. (c) and (d) Comparison of c evaluated using DMRG and correlation matrix at the free fermionic limit ($\phi = 0$) as a function of t_2 for different system sizes. (d) Dependence of c evaluated at $t_2 = -1, \phi = 0$ for different system sizes and bond dimension. Even at the free fermion limit, to capture the $c = 2$ phase one needs to have a significantly large bond dimension.

The behavior of c near the $\phi = 0$ limit can be understood by comparing the results of DMRG with that obtained by calculating entanglement entropy using the correlation matrix [84–87] ($C_{ij} = \langle c_i^\dagger c_j \rangle$) where the expectation is taken over the occupied states. The value of central charge calculated using this is shown in Fig. 17.

APPENDIX E: DETAILS OF THE BOSONIZATION

The interaction term is given by

$$\tilde{H}_{\rm int} = -t_2 \sum_{k_1,k_2,k_3,k_4} \delta_{k_1+k_2-k_3-k_4}(e^{i\phi}-1)e^{i(-k_2+k_3+2k_4)} \times \left[:c_{k_1}^\dagger c_{k_4}:: c_{k_2}^\dagger c_{k_3}: - :c_{k_1}^\dagger c_{k_3}:: c_{k_2}^\dagger c_{k_4}: \right] + \text{H.c.}, \tag{E1}$$

where the normal ordering is done about the HF ground state. Identifying the slow modes, one finds two essential scattering contributions: (i) Forward scattering and (ii) Umklapp scattering. Defining

$$\rho_R(q) = \sum_{q_1} :c_{q_1 R}^\dagger c_{q_1+qR}:, \tag{E2}$$

$$\rho_R(x) = \sum_q e^{iqx}\rho_R(q), \tag{E3}$$

forward scattering contribution is

$$\tilde{H}_{\rm int}^{\rm Fow} = V\int dx[(\rho_R+\rho_L)^2 - (\rho_R-\rho_L)^2] = V\int dx[(\partial_x\Phi)^2 - (\partial_x\Theta)^2], \tag{E4}$$

where $V = 4t_2[\cos(\phi + 2k_o) - \cos(2k_o)]$. For the Umklapp process the contribution is

$$\tilde{H}_{\rm int}^{\rm Ump} = -\lambda\int dx \cos 4\Phi, \tag{E5}$$

with $\lambda = -2V$, which is the characteristic doubled vortex tunneling process at half-filling.

1. Characterisation of the phases in the bosonic language

While most of our discussion of the gapless phases has been in terms of TLL, a quantity worth investigating is the expectation value of $\langle n_k^b \rangle \equiv \langle b_k^\dagger b_k \rangle$ which is expectation of each of the occupancy of the kth mode in bosonic language. Figure 18 shows this for various values of ϕ and t_2 [$\langle n_b(k)\rangle = \langle b^\dagger(k)b(k)\rangle = \frac{1}{L}\sum_{i,j}\exp ik(i-j)\langle S_i^+ S_j^-\rangle$]. Clearly the TLL phase is equivalently a power-law superfluid as pointed in the main text. The shifted center of the Fermi sea in TLL manifests as again a shifted k point where the superfluid $\langle n_b(k)\rangle$ peaks.

2. Characterization of the $c = 1$ TLL phase: Luttinger parameters from DMRG study

To characterize the $c = 1$ TLL, it is particularly useful to calculate the fermion-fermion correlation function in this system. In the regime when the $\langle n(k)\rangle$ shows "two" Fermi surfaces, i.e., $c = 1$ TLL,

$$C(r) = \frac{1}{L}\sum_i \langle c_i^\dagger c_{i+r}\rangle = \frac{1}{2\pi}\int_{-\pi}^{\pi} dk \langle n(k)\rangle e^{-ikr}. \tag{E6}$$

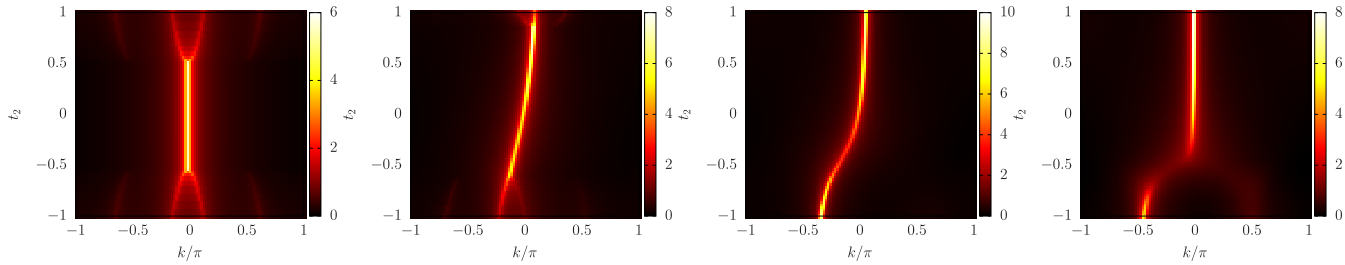

FIG. 18. Bosonic occupancy: Bosonic $\langle n_b(k)\rangle$ as a function of k and t_2 for different values of $\phi = 0.0$, 1.0, 2.0, and 3.0 ($L = 62$).

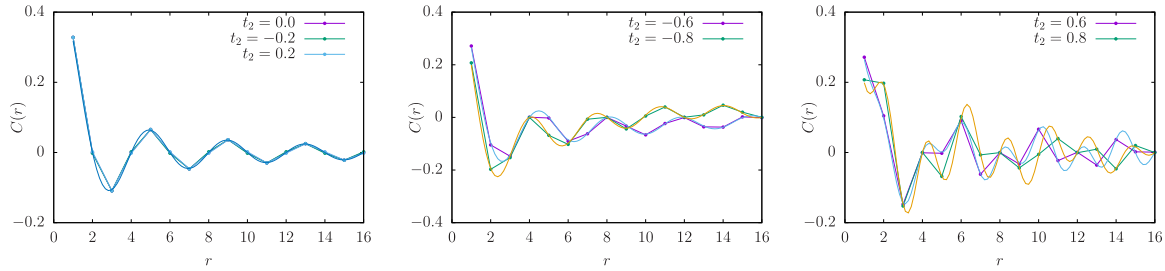

FIG. 19. Fermionic correlator: $C(r)$ has a function of r for $\phi = 0$ for different values of t_2. The numerical values from DMRG are the points. The continuous lines are the expressions shown near Eq. (E8) for the appropriate parameters.

For the case when $\phi = 0$ and $-0.5 \leqslant t_2 \leqslant 0.5$, such that there is a filled Fermi sea between $-\frac{\pi}{2} \leqslant k \leqslant \frac{\pi}{2}$,

$$C(r) = \frac{\sin(\pi r/2)}{\pi r}. \tag{E7}$$

For $|t_2| \geqslant 0.5$, $C(r)$ shows an oscillating behavior due to new Fermi wave vectors. In particular, for $t_2 < -0.5$ we have two Fermi seas, one between $k_F^{L+} \leqslant k \leqslant k_F^{R+}$ and the other between $k_F^{L-} \leqslant k \leqslant k_F^{R-}$. In this regime

$$C(r) = \frac{2\cos\left(\arccos\left(\frac{t_1}{2\sqrt{2}|t_2|}\right)r\right)\sin\left(\frac{\pi}{4}r\right)}{\pi r}. \tag{E8}$$

Similar calculations can be done for for $t_2 > 0.5$ (see Fig. 19). In the presence of the interactions ($\phi \neq 0$) the long wavelength scaling of the correlation function changes from $\sim\frac{1}{r}$ to $\frac{1}{r^\eta}$ where η can be related to the Luttinger parameter [75]. In $c = 1$ TLL, which is the region of $-0.5 < t_2 < 0.5$ and when $\phi \neq 0$, we fit $C(r)$ to a functional form

$$C(r) \sim \frac{\cos(k_o x)\sin\left(\frac{\pi}{2}x\right)}{\pi x^\eta}, \tag{E9}$$

where both η and k_o are fitting parameters. The intention is to capture the shift in the Fermi sea (k_o) and the Luttinger parameter (K) where K is related to η via $\eta = \frac{1}{2}(K + \frac{1}{K})$. A comparison of k_o obtained by above and the Hartree-Fock solution is shown in Fig. 15 for bench marking.

[1] A. Y. Kitaev, Phys. Usp. **44**, 131 (2001).
[2] J. Alicea, Rep. Prog. Phys. **75**, 076501 (2012).
[3] V. Mourik, K. Zuo, S. M. Frolov, S. Plissard, E. P. Bakkers, and L. P. Kouwenhoven, Science **336**, 1003 (2012).
[4] J. M. Leinaas and J. Myrheim, Il Nuovo Cimento B (1971–1996) **37**, 1 (1977).
[5] E. H. Lieb and W. Liniger, Phys. Rev. **130**, 1605 (1963).
[6] A. Kundu, Phys. Rev. Lett. **83**, 1275 (1999).
[7] V. Pasquier, *Integrable Models and Strings* (Springer, Berlin, 1994), pp. 36–48.
[8] Z. N. C. Ha, Phys. Rev. Lett. **73**, 1574 (1994).
[9] Z. Ha, Nucl. Phys. B **435**, 604 (1995).
[10] T. Keilmann, S. Lanzmich, I. McCulloch, and M. Roncaglia, Nat. Commun. **2**, 361 (2011).
[11] C. Sträter, S. C. L. Srivastava, and A. Eckardt, Phys. Rev. Lett. **117**, 205303 (2016).
[12] S. Greschner and L. Santos, Phys. Rev. Lett. **115**, 053002 (2015).
[13] L. Cardarelli, S. Greschner, and L. Santos, Phys. Rev. A **94**, 023615 (2016).
[14] S. Greschner, L. Cardarelli, and L. Santos, Phys. Rev. A **97**, 053605 (2018).
[15] C. Aneziris, A. P. Balachandran, and D. Sen, Int. J. Mod. Phys. A **6**, 4721 (1991).
[16] T. Posske, B. Trauzettel, and M. Thorwart, Phys. Rev. B **96**, 195422 (2017).
[17] M. Frau, A. Lerda, and S. Sciuto, arXiv:hep-th/9407161.
[18] M. El Baz and Y. Hassouni, Int. J. Mod. Phys. A **18**, 3015 (2003).
[19] F. D. M. Haldane, Phys. Rev. Lett. **67**, 937 (1991).
[20] Y.-S. Wu, Phys. Rev. Lett. **73**, 922 (1994).
[21] M. V. N. Murthy and R. Shankar, Phys. Rev. Lett. **73**, 3331 (1994).
[22] F. A. An, E. J. Meier, and B. Gadway, Sci. Adv. **3**, e1602685 (2017).
[23] F. A. An, E. J. Meier, J. Ang'ong'a, and B. Gadway, Phys. Rev. Lett. **120**, 040407 (2018).
[24] F. A. An, E. J. Meier, and B. Gadway, Phys. Rev. X **8**, 031045 (2018).
[25] E. J. Meier, F. A. An, A. Dauphin, M. Maffei, P. Massignan, T. L. Hughes, and B. Gadway, Science **362**, 929 (2018).
[26] M. T. Batchelor, X.-W. Guan, and N. Oelkers, Phys. Rev. Lett. **96**, 210402 (2006).
[27] H. Guo, Y. Hao, and S. Chen, Phys. Rev. A **80**, 052332 (2009).
[28] M. Eckholt and J. J. García-Ripoll, New J. Phys. **11**, 093028 (2009).
[29] M. Eckholt and J. J. García-Ripoll, Phys. Rev. A **77**, 063603 (2008).
[30] J. Arcila-Forero, R. Franco, and J. Silva-Valencia, Phys. Rev. A **94**, 013611 (2016).
[31] W. Zhang, S. Greschner, E. Fan, T. C. Scott, and Y. Zhang, Phys. Rev. A **95**, 053614 (2017).
[32] F. Lange, S. Ejima, and H. Fehske, Phys. Rev. Lett. **118**, 120401 (2017).
[33] F. Lange, S. Ejima, and H. Fehske, Phys. Rev. A **95**, 063621 (2017).
[34] J. Arcila-Forero, R. Franco, and J. Silva-Valencia, Phys. Rev. A **97**, 023631 (2018).

[35] Z.-W. Zuo, G.-L. Li, and L. Li, Phys. Rev. B **97**, 115126 (2018).
[36] S. Kolkowitz, S. Bromley, T. Bothwell, M. Wall, G. Marti, A. Koller, X. Zhang, A. Rey, and J. Ye, Nature (London) **542**, 66 (2017).
[37] G. Jotzu, M. Messer, F. Görg, D. Greif, R. Desbuquois, and T. Esslinger, Phys. Rev. Lett. **115**, 073002 (2015).
[38] F. Görg, K. Sandholzer, J. Minguzzi, R. Desbuquois, M. Messer, and T. Esslinger, arXiv:1812.05895.
[39] W. Xu, W. Morong, H.-Y. Hui, V. W. Scarola, and B. DeMarco, Phys. Rev. A **98**, 023623 (2018).
[40] M. Lebrat, P. Grišins, D. Husmann, S. Häusler, L. Corman, T. Giamarchi, J.-P. Brantut, and T. Esslinger, Phys. Rev. X **8**, 011053 (2018).
[41] M. Lebrat, S. Häusler, P. Fabritius, D. Husmann, L. Corman, and T. Esslinger, arXiv:1902.05516.
[42] G. Salomon, J. Koepsell, J. Vijayan, T. A. Hilker, J. Nespolo, L. Pollet, I. Bloch, and C. Gross, Nature (London) **565**, 56 (2019).
[43] B. Song, L. Zhang, C. He, T. F. J. Poon, E. Hajiyev, S. Zhang, X.-J. Liu, and G.-B. Jo, Sci. Adv. **4**, eaao4748 (2018).
[44] J. H. Han, J. H. Kang, and Y. Shin, Phys. Rev. Lett. **122**, 065303 (2019).
[45] M. Mancini, G. Pagano, G. Cappellini, L. Livi, M. Rider, J. Catani, C. Sias, P. Zoller, M. Inguscio, M. Dalmonte, and L. Fallani, Science **349**, 1510 (2015).
[46] L. F. Livi, G. Cappellini, M. Diem, L. Franchi, C. Clivati, M. Frittelli, F. Levi, D. Calonico, J. Catani, M. Inguscio, and L. Fallani, Phys. Rev. Lett. **117**, 220401 (2016).
[47] J. H. Kang, J. H. Han, and Y.-i. Shin, arXiv:1902.10304.
[48] J. H. Kang, J. H. Han, and Y. Shin, Phys. Rev. Lett. **121**, 150403 (2018).
[49] M. E. Foglio and L. M. Falicov, Phys. Rev. B **20**, 4554 (1979).
[50] L. Arrachea and A. A. Aligia, Phys. Rev. Lett. **73**, 2240 (1994).
[51] J. de Boer, V. E. Korepin, and A. Schadschneider, Phys. Rev. Lett. **74**, 789 (1995).
[52] J. Vidal and B. Douçot, Phys. Rev. B **65**, 045102 (2001).
[53] I. Lifshitz *et al.*, Sov. Phys. JETP **11**, 1130 (1960).
[54] Y. M. Blanter, M. Kaganov, A. Pantsulaya, and A. Varlamov, Phys. Rep. **245**, 159 (1994).
[55] Y. Yamaji, T. Misawa, and M. Imada, J. Phys. Soc. Jpn. **75**, 094719 (2006).
[56] M. Rodney, H. F. Song, S.-S. Lee, K. Le Hur, and E. S. Sørensen, Phys. Rev. B **87**, 115132 (2013).
[57] W. Ketterle and M. W. Zwierlein, La Rivista Del Nuovo Cimento **5**, 247 (2008).
[58] S. Giorgini, L. P. Pitaevskii, and S. Stringari, Rev. Mod. Phys. **80**, 1215 (2008).
[59] Y. Hao, Y. Zhang, and S. Chen, Phys. Rev. A **79**, 043633 (2009).
[60] Y. Hao and S. Chen, Phys. Rev. A **86**, 043631 (2012).
[61] S. Sarkar, Phys. Rev. B **75**, 014528 (2007).
[62] C. D. Batista, F. Lema, and A. A. Aligia, Phys. Rev. B **52**, 6223 (1995).
[63] L. Arrachea, A. A. Aligia, and E. Gagliano, Phys. Rev. Lett. **76**, 4396 (1996).
[64] G. Santoro, M. Airoldi, N. Manini, E. Tosatti, and A. Parola, Phys. Rev. Lett. **74**, 4039 (1995).
[65] Y.-C. He, S. Bhattacharjee, R. Moessner, and F. Pollmann, Phys. Rev. Lett. **115**, 116803 (2015).
[66] ITensor, http://itensor.org/.
[67] P. Calabrese and J. Cardy, J. Phys. A **42**, 504005 (2009).
[68] T. Mishra, R. V. Pai, S. Mukerjee, and A. Paramekanti, Phys. Rev. B **87**, 174504 (2013).
[69] A. Dhar, T. Mishra, R. V. Pai, S. Mukerjee, and B. P. Das, Phys. Rev. A **88**, 053625 (2013).
[70] C. K. Majumdar and D. K. Ghosh, J. Math. Phys. **10**, 1399 (1969).
[71] C. K. Majumdar and D. K. Ghosh, J. Math. Phys. **10**, 1388 (1969).
[72] S.-J. Gu, Int. J. Mod. Phys. B **24**, 4371 (2010).
[73] M. Dalmonte, J. Carrasquilla, L. Taddia, E. Ercolessi, and M. Rigol, Phys. Rev. B **91**, 165136 (2015).
[74] J. Carrasquilla, S. R. Manmana, and M. Rigol, Phys. Rev. A **87**, 043606 (2013).
[75] S. Sachdev, *Quantum Phase Transitions* (Cambridge University Press, Cambridge, 2011).
[76] S. Ray, S. Mukerjee, and V. B. Shenoy, Ann. Phys. **384**, 71 (2017).
[77] O. M. Sule, H. J. Changlani, I. Maruyama, and S. Ryu, Phys. Rev. B **92**, 075128 (2015).
[78] D. Baeriswyl and L. Degiorgi, *Strong Interactions in Low Dimensions* (Springer Science & Business Media, New York, 2005), Vol. 25.
[79] S. Sachdev, Physica A (Amsterdam) **313**, 252 (2002).
[80] M. Sitte, A. Rosch, J. S. Meyer, K. A. Matveev, and M. Garst, Phys. Rev. Lett. **102**, 176404 (2009).
[81] T. Meng, M. Dixit, M. Garst, and J. S. Meyer, Phys. Rev. B **83**, 125323 (2011).
[82] M. Di Liberto, C. E. Creffield, G. I. Japaridze, and C. Morais Smith, Phys. Rev. A **89**, 013624 (2014).
[83] S. K. Ghosh, S. Greschner, U. K. Yadav, T. Mishra, M. Rizzi, and V. B. Shenoy, Phys. Rev. A **95**, 063612 (2017).
[84] M.-C. Chung and I. Peschel, Phys. Rev. B **64**, 064412 (2001).
[85] S.-A. Cheong and C. L. Henley, Phys. Rev. B **69**, 075111 (2004).
[86] I. Peschel, J. Phys. A **36**, L205 (2003).
[87] G. Vidal, J. I. Latorre, E. Rico, and A. Kitaev, Phys. Rev. Lett. **90**, 227902 (2003).